Chapter 6

Observation of Transverse Wobbling Motion and Chiral Bands in ^{119}I

6.1 Introduction

The shape of a nucleus provides vital information about its internal structure and forces, making it one of the most crucial properties for understanding atomic and nuclear phenomena. The nuclei above the $Z = 50$ shell are well known to exhibit various properties related to different shapes. The Sb nuclei with $Z = 51$ and $N \approx 66$ exhibit spherical single-particle structures at low spins, whereas regular rotational structures are observed at higher excitation energy [189]. The Te nuclei are mainly known for the vibrational character near the ground state; however, the pure vibrational character in some nuclei has been interpreted to be a result of the interplay between γ soft and vibrational character [147–149]. Iodine nuclei ($Z = 53$) lie in a transitional region between the vibration-like Te ($Z = 52$) and the deformed rotor Xe ($Z = 54$) [190]. The available small number of valence particles or holes outside the magic core of Sn nuclei are sufficient to break the spherical symmetry and drive the nucleus towards axial or triaxial deformation. In recent times, the triaxial nuclear shapes have gained much interest because of different structural

phenomena arising from the unequal nuclear mass distribution along the three principal axes. Observation of wobbling phenomena [47–57, 59, 60, 191], existence of γ bands [8, 192, 193] and observation of time reversal chiral doublet bands [39, 40, 194, 195] are the prominent experimental signatures of triaxiality.

Chirality has been reported in many nuclei of mass region $A\simeq$120-130 [39, 40, 194, 195]. Interestingly, in the case of iodine isotopes, chiral-like partner doublet bands have been suggested in ^{120,123}I [194, 195]. The observation of doublet structure in Z = 53 iodine can be regarded as induced by the coupling of the triaxial γ soft core with the proton and neutron in the same $h_{11/2}$ orbital. However, the observation of chiral-like doublet bands needs further theoretical investigations in case ^{123}I [194]. Therefore, it would be interesting to search for chiral-like doublet bands in ^{119}I within a relevant theoretical model. The other signature of triaxiality, i.e., wobbling, has been reported in many nuclei of these mass regions (^{130,133}Ba [55, 56], ^{133}La [196], and ^{125,127}Xe[53, 54]). However, the criterion requiring the simultaneous existence of both signatures of triaxiality within a single nucleus was considered questionable. Theoretically, chiral wobbler in nuclei was first suggested by T. Koike *et al.* by using a quantum particle rotor model (PRM) [197]. Recently, the first evidence of chiral wobbler was observed in ^{74}Br based on the same configurations. It is interesting to note that, except for ^{133}La, no other nuclei in this mass region have been reported for the existence of chiral and wobbler modes [57, 196], but unlike ^{74}Br, both modes were observed to evolve from different configurations. It motivates further studies of the coexistence of multiple symmetries in a single nucleus. The negative-parity yrast band in ^{119}I is built on the $\pi h_{11/2}[550]1/2^-$ configuration and the properties of $\pi h_{11/2}$ yrast band mostly follow the ground state band in ^{120}Xe rather than those of Te nuclei [189]. The occupancy of this orbital stabilizes a prolate quadrupole deformation of $\beta \approx 0.25$ [198]. Hence, ^{119}I can be a good candidate to study the coexistence of multiple symmetries in a single nucleus.

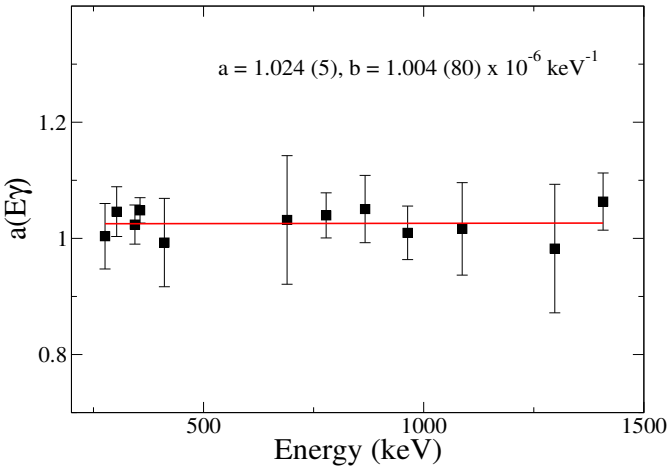

Figure 6.1 The asymmetry correction factor a(E_γ) at different γ-ray energies. The solid line corresponds to a linear fit of the data.

6.2 Experimental Details

The excited states of ^{119}I were populated through ^{109}Ag(^{13}C, 3nγ)^{119}I reaction at a beam energy of 54 MeV. The ^{13}C beam, provided by the 14UD pelletron accelerator (TIFR), was incident on a ^{109}Ag target of thickness 1.62 mg/cm^2 backed with 10.5 mg/cm^2 of Au. The emitted γ rays were detected in the Indian National Gamma Array (INGA), which consisted of 18 Compton-suppressed clover HPGe detectors. A total number of 1.62×10^9 γ-γ coincidence events were collected into a two-dimensional matrix format by using RADWARE software [141]. During the experiment, a total of eighteen clover detectors were placed at different angles, three each at 157°, 140°, 115°, and 40°, four at 90 ° and two at 65°. The spin and parity assignments were made on the basis of the directional correlation ratio and polarization asymmetry measurements. More details of the measurement techniques have been discussed in Chapter 2. In the present work, 157° angle was used to determine the directional correlation ratio as backward angle. For the

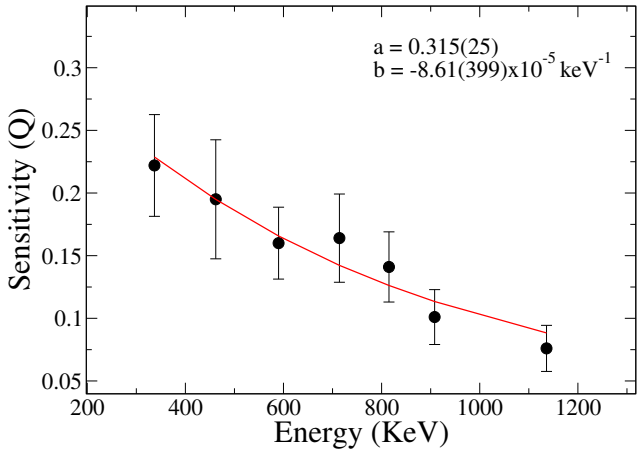

Figure 6.2 polarization sensitivity of the clover detector placed at the 90° of the INGA array in the present experiment.

linear polarization measurement, the geometrical asymmetry factor $a(E_\gamma)$ and polarization sensitivity measurements are shown in Fig. 6.1, 6.2, and Table 6.1.

Table 6.1 The known $E2$ transitions of ^{119}I, produced in the present experiment, for which the value of $Q(E_\gamma)$ was measured. These values of $Q(E_\gamma)$ are used to obtain the coefficients a and b as shown in Fig. 6.2.

Nucleus	$E\gamma$ (keV)	a_2	a_4	$P(\theta)$	$\triangle_{asym}$	Q
^{119}I	337.0	0.32 (5)	-0.04 (8)	0.55 (8)	0.123 (3)	0.22 (4)
	461.7	0.29 (5)	-0.03 (8)	0.49 (8)	0.096 (3)	0.20 (5)
	590.5	0.31 (5)	-0.05 (9)	0.52 (9)	0.084 (3)	0.16 (3)
	714.3	0.26 (5)	-0.07 (8)	0.41 (8)	0.067 (5)	0.16 (4)
	814.6	0.29 (6)	-0.04 (8)	0.48 (0)	0.069 (6)	0.14 (3)
	908.2	0.29 (6)	-0.07 (9)	0.47 (10)	0.048 (10)	0.10 (2)
	1136.2	0.28 (6)	-0.08 (10)	0.44 (10)	0.034 (15)	0.07 (2)

6.3 Results and Discussions

The nucleus ^{119}I was earlier studied by various groups [152, 189, 198]. The work of Kostov *et al.* mostly focuses on the isomeric decay patterns of prolate deformed $11/2^-$

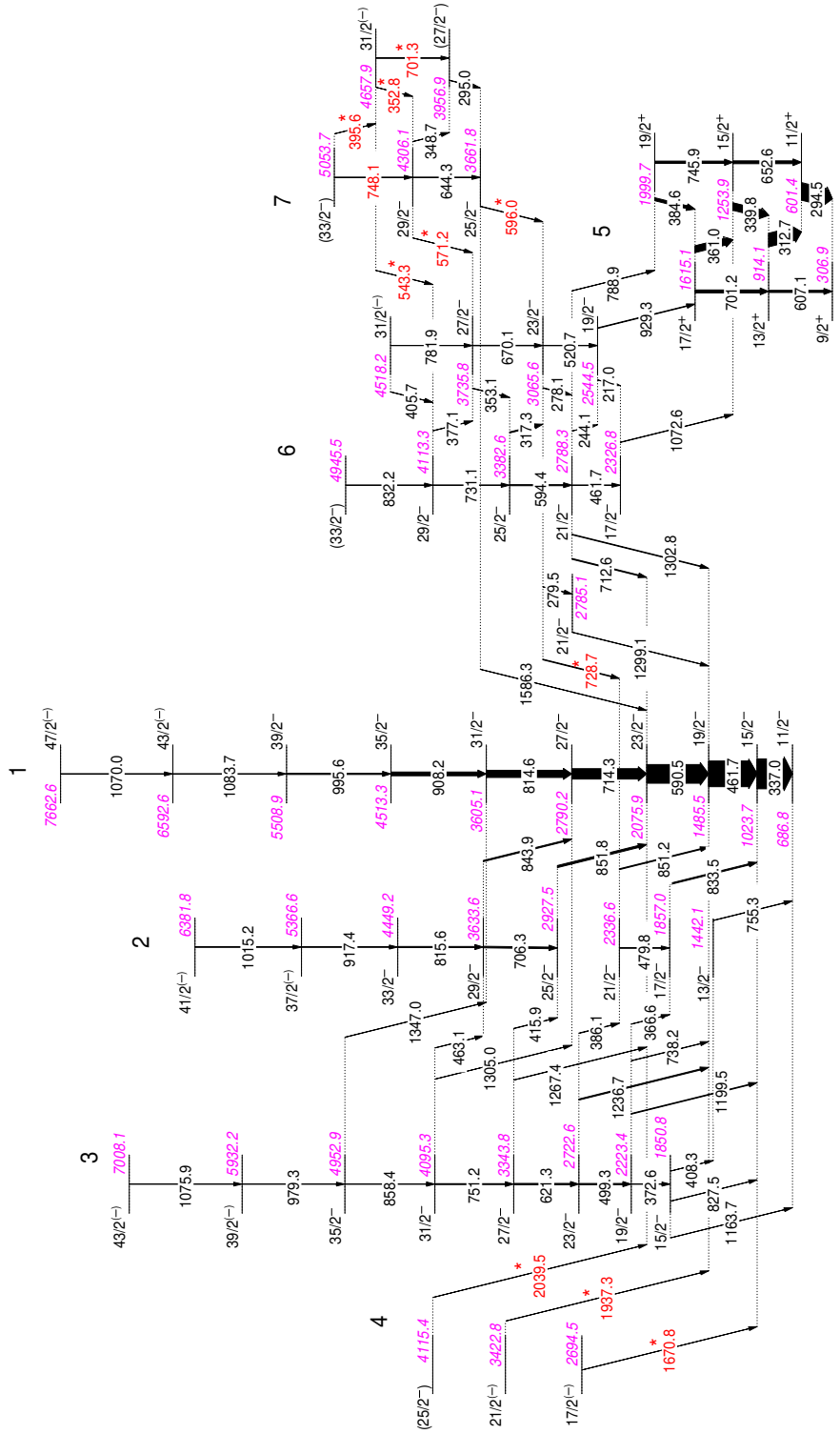

Figure 6.3 Partial level scheme of ^{119}I based on present work and previous work [152, 198].

band head of presently shown band 1, whereas Paul *et al.* has emphasized shape evolution as a function of angular momentum in band 1. According to the study by Paul *et al.* the states below $I = 39/2\,\hbar$ is associated with prolate shape based on $\pi h_{11/2}$ orbital whereas $I = 43/2^-$ attains non-collective oblate minima with a fully aligned configuration $\pi[h_{11/2} \otimes g^2_{7/2}]_{23/2^-} \otimes \nu[h^2_{11/2}]_{10^+}$. Henceforth, band 1 regains the collectivity, and the rotational structure was realized till $I = 63/2^-$. The bands 1, 2, and 3 were previously analyzed in detail by Törmänen *et al.* [189]. These bands were also observed in the present work and the placement of γ transitions along with the spin-parity assignments to the levels completely agrees with the previous results. The detailed level scheme is shown in Fig. 6.3, whereas the level energy, γ-ray energy, initial and final spin states, multipolarity etc., are shown in Table 6.2.

Table 6.2 List of initial states (E_i) and energies of γ rays (E_γ), spins, relative intensity (I_γ), R_{DCO} values, linear polarization asymmetry (Δ_{asym}), multipole mixing ratio ($\delta_{E2/M1}$), and multipolarity ($E\lambda/M\lambda$) of the γ transition in ^{119}I.

$E_i^{\#}$(keV)	E_γ (keV)	$I_i \rightarrow I_f$	$I_\gamma{}^\dagger$	R_{DCO}	Δ_{asym}	$\delta_{E2/M1}$	$E\lambda/M\lambda$
601.4 (2)	294.5 (2)	$11/2^+ \rightarrow 9/2^+$	56.5 (28)	0.79 (6)[a]	-0.144 (8)	0.29^{+4}_{-13} [p]	$M1$+$E2$
914.1 (2)	312.7 (2)	$13/2^+ \rightarrow 11/2^+$	43.9 (22)	0.82 (6)[a]	-0.121 (10)	0.20^{+11}_{-4} [p]	$M1$+$E2$
	607.1 (3)	$13/2^+ \rightarrow 9/2^+$	7.39 (55)	1.10 (8)[a]	0.074 (10)	-	$E2$
1023.7 (6)	337.0 (2)	$15/2^- \rightarrow 11/2^-$	100.0 (5)	1.08 (7)[b]	0.123 (5)	-	$E2$
1253.9 (3)	339.8 (2)	$15/2^+ \rightarrow 13/2^+$	24.5 (13)	0.86 (7)[a]	-0.131 (12)	0.28^{+10}_{-8} [p]	$M1$+$E2$
	652.6 (3)	$15/2^+ \rightarrow 11/2^+$	9.76 (58)	0.97 (6) [a]	0.12 (5)		$E2$
1442.1 (7)	755.3 (2)	$13/2^- \rightarrow 11/2^-$	-	-	-		-
1485.5 (6)	461.7 (2)	$19/2^- \rightarrow 15/2^-$	87.4 (44)	1.02 (7)[c]	0.096 (5)		$E2$
1615.1 (3)	361.0 (2)	$17/2^+ \rightarrow 15/2^+$	22.4 (12)	0.74 (5)[d]	-0.107 (14)	0.19^{+9}_{-6} [p]	$M1$+$E2$
	701.2 (3)	$17/2^+ \rightarrow 13/2^+$	10.2 (6)	1.10 (8)[e]	0.057 (9)		$E2$
1850.8 (7)	408.3[l] (4)	$15/2^- \rightarrow 13/2^-$	0.25 (10)	-	-		-
	827.5[l] (6)	$15/2^- \rightarrow 15/2^-$	0.30 (6)	-	-		-
	1163.7[l] (6)	$15/2^- \rightarrow 11/2^-$	0.25 (7)	-	-		-

E_i[#](keV)	E_γ (keV)	$I_i \rightarrow I_f$	I_γ[†]	R_{DCO}	Δ_{asym}	$\delta_{E2/M1}$	$E\lambda/M\lambda$
1857.0 (7)	833.5 (4)	$17/2^- \rightarrow 15/2^-$	4.48 (31)	0.29 (3)[c]	0.022 (12)	-2.40^{+64}_{-43} [p]	$M1+E2$
1999.7 (3)	384.6 (2)	$19/2^+ \rightarrow 17/2^+$	9.94 (57)	0.75 (6)[d]	-0.12 (1)	0.20^{+10}_{-6} [p]	$M1+E2$
	745.9 (2)	$19/2^+ \rightarrow 15/2^+$	8.2 (5)	0.95 (7)[d]	0.089 (2)		$E2$
2075.9 (6)	590.5 (2)	$23/2^- \rightarrow 19/2^-$	64.1 (33)	1.08 (8)[c]	0.084 (5)		$E2$
2223.4 (7)	366.6 (4)	$19/2^- \rightarrow 17/2^-$	0.74 (12)	0.30 (3)[f]	0.045 (27)	-2.49^{+83}_{-63} [p]	$M1+E2$
	372.6 (3)	$19/2^- \rightarrow 15/2^-$	0.71 (21)	1.02 (9)[f]	0.11 (5)		$E2$
	738.2 (5)	$19/2^- \rightarrow 19/2^-$	1.10 (7)	0.69 (6)[f]	-0.052 (35)	1.63^{+78}_{-40} [p]	$M1+E2$
	1199.5 (5)	$19/2^- \rightarrow 15/2^-$	2.46 (24)	1.03 (8)[c]	0.12 (3)		$E2$
2326.8 (5)	1072.6 (5)	$17/2^- \rightarrow 15/2^+$	1.12 (14)	0.71 (9)[d]	0.045 (31)	0.12^{+11}_{-7} [p]	$E1$
2336.6 (6)	479.8 (4)	$21/2^- \rightarrow 17/2^-$	0.80 (13)	1.10(11)[c]	0.10 (5)		$E2$
	851.2[m] (5)	$21/2^- \rightarrow 19/2^-$	3.03 (39)	-	-	-	
2544.5 (5)	217.0[l] (6)	$19/2^- \rightarrow 17/2^-$	-	-	-		-
	929.3 (5)	$19/2^- \rightarrow 17/2^+$	2.05 (16)	0.66 (5)[d]	0.033 (21)	0.09^{+7}_{-6} [p]	$E1$
2694.5 (10)	1670.8[*,m] (6)	$17/2^{(-)} \rightarrow 15/2^-$	0.30 (5)	0.55 (7)[c]	-		$(M1)$
2722.6 (6)	386.1 (3)	$23/2^- \rightarrow 21/2^-$	1.41 (20)	0.67 (5)[b]	-0.11 (4)	0.11^{+11}_{-7} [p]	$M1+E2$
	499.3 (3)	$23/2^- \rightarrow 19/2^-$	4.46 (31)	0.95 (7)[c]	0.08 (3)		$E2$
	1236.7 (5)	$23/2^- \rightarrow 19/2^-$	3.75 (25)	0.94 (7)[c]	0.041 (20)		$E2$
2785.1 (7)	1299.1 (5)	$21/2^- \rightarrow 19/2^-$	0.92 (12)	0.54 (7)[b]	-0.041 (33)		$M1$
2788.3 (5)	244.1[l] (6)	$21/2^- \rightarrow 19/2^-$	0.27 (12)	-	-		-
	461.7[m] (5)	$21/2^- \rightarrow 17/2^-$	0.85 (21)	-	-		-
	712.6[m] (4)	$21/2^- \rightarrow 23/2^-$	3.10 (5)	-	-		
	788.9[m] (5)	$21/2^- \rightarrow 19/2^+$	0.64 (17)	-	-		-
	1302.8 (5)	$21/2^- \rightarrow 19/2^-$	2.23 (19)	0.55 (5)[c]	-0.058 (33)		$M1$
2790.2 (7)	714.3 (3)	$27/2^- \rightarrow 23/2^-$	35.7 (18)	1.07 (8)[c]	0.067(6)		$E2$
2927.5 (7)	851.8 (5)	$25/2^- \rightarrow 23/2^-$	7.12 (58)	0.31 (3)[i]	0.025 (10)	-2.57^{+59}_{-42} [p]	$M1+E2$
3065.6 (5)	278.1 (4)	$23/2^- \rightarrow 21/2^-$	1.70 (13)	0.68 (6)[h]	-0.14 (5)	0.10^{+15}_{-6} [p]	$M1+E2$
	279.5[m,l] (7)	$23/2^- \rightarrow 21/2^-$	0.82 (8)	-	-		-

$E_i^{\#}$(keV)	E_γ (keV)	$I_i \rightarrow I_f$	$I_\gamma^{\dagger}$	R_{DCO}	Δ_{asym}	$\delta_{E2/M1}$	$E\lambda/M\lambda$
	520.7 (3)	$23/2^- \rightarrow 19/2^-$	1.71 (14)	0.94 (8)[g]	0.11 (4)		$E2$
	728.7[*,n] (5)	$23/2^- \rightarrow 21/2^-$	2.30 (30)	-	-		-
3343.8 (7)	415.9[m] (6)	$27/2^- \rightarrow 25/2^-$	1.11 (22)	0.63 (5)[h]	-	0.11^{+8}_{-4} [q]	($M1$)
	621.3 (3)	$27/2^- \rightarrow 23/2^-$	4.88 (32)	1.10 (8)[c]	0.074 (21)		$E2$
	1267.4[m] (6)	$27/2^- \rightarrow 23/2^-$	0.61 (9)	0.95 (9)[c]			($E2$)
3382.6 (6)	317.3 (4)	$25/2^- \rightarrow 23/2^-$	3.45 (26)	0.82 (7)[h]	-0.13 (3)	0.18^{+17}_{-6} [p]	$M1$+$E2$
	594.4 (3)	$25/2^- \rightarrow 21/2^-$	3.66 (30)	0.94 (14)[r]	-		($E2$)
3422.8 (10)	1937.3[*,m] (7)	$21/2^{(-)} \rightarrow 19/2^-$	0.40 (6)	0.62 (6)[c]	-		($M1$)
3605.1 (7)	814.6 (3)	$31/2^- \rightarrow 27/2^-$	24.7 (13)	1.01 (8)[c]	0.069 (7)		$E2$
3633.6 (7)	706.3 (3)	$29/2^- \rightarrow 25/2^-$	5.48 (36)	1.10 (9)[c]	0.042 (18)		$E2$
	843.9 (4)	$29/2^- \rightarrow 27/2^-$	4.18 (31)	0.37 (3)[c]	0.025 (14)	-3.47^{+54}_{-74} [p]	$M1$+$E2$
3661.8 (6)	596.0[*,m] (4)	$25/2^- \rightarrow 23/2^-$	1.24 (21)	0.80 (12) [s]	-		-
	1586.3 (5)	$25/2^- \rightarrow 23/2^-$	0.65 (7)	0.55 (5)[b]	-0.082 (80)		$M1$
3735.8 (6)	353.1[m] (4)	$27/2^- \rightarrow 25/2^-$	1.45 (17)	0.74 (8)[j]	-	0.17^{+7}_{-6} [q]	$M1$+$E2$
	670.1 (3)	$27/2^- \rightarrow 23/2^-$	1.70 (26)	0.99 (9)[g]	0.069 (29)		$E2$
3956.9 (7)	295.0[o] (5)	$(27/2^-) \rightarrow 25/2^-$	1.05 (37)	-	-		-
4095.3 (7)	463.1[m] (5)	$31/2^- \rightarrow 29/2^-$	0.57 (20)	-	-		-
	751.2 (4)	$31/2^- \rightarrow 27/2^-$	3.15 (26)	1.00 (9)[h]	0.11 (4)		$E2$
	1305.0[m] (3)	$31/2^- \rightarrow 27/2^-$	0.40 (8)	1.05 (20)[h]	-		($E2$)
4113.3 (6)	377.1 (4)	$29/2^- \rightarrow 27/2^-$	1.02 (21)	0.71 (10)[h]	-	0.19^{+11}_{-12} [q]	$M1$+$E2$
	731.1 (4)	$29/2^- \rightarrow 25/2^-$	1.6 (26)	1.1 (9)[h]	0.09 (4)		$E2$
4115.4 (11)	2039.5[*,l] (8)	$(25/2^-) \rightarrow 23/2^-$	0.50 (9)	-	-		
4306.1 (7)	348.7[m] (6)	$29/2^- \rightarrow (27/2^-)$	0.58 (21)	0.66 (9) [h]	-	0.13^{+5}_{-6} [q]	$M1$+$E2$
	571.2[*,l] (5)	$29/2^- \rightarrow 27/2^-$	0.40 (20)	-	-	-	-
	644.3 (6)	$29/2^- \rightarrow 25/2^-$	0.73 (20)	1.12(12)[s]	0.45 (35)		$E2$
4449.2 (8)	815.6 (3)	$33/2^- \rightarrow 29/2^-$	4.00 (30)	1.08 (7)[i]	0.12 (3)		$E2$
4513.3 (8)	908.2 (4)	$35/2^- \rightarrow 31/2^-$	13.04 (73)	1.07 (8)[c]	0.048 (11)		$E2$

E_i[#](keV)	E_γ (keV)	$I_i \rightarrow I_f$	I_γ[†]	R_{DCO}	Δ_{asym}	$\delta_{E2/M1}$	$E\lambda/M\lambda$
4518.2 (7)	405.7[m] (5)	$31/2^{(-)} \rightarrow 29/2^-$	0.75 (19)	0.66 (7)[k]	-	0.12^{+5}_{-4} [q]	$M1$+$E2$
	781.9[m] (4)	$31/2^{(-)} \rightarrow 27/2^-$	0.78 (19)	1.15 (17)[h]	-		($E2$)
4657.9 (7)	352.8[*,m] (7)	$31/2^{(-)} \rightarrow 29/2^-$	0.57 (27)	0.67 (12)[k]	-	0.12^{+10}_{-12} [q]	$M1$+$E2$
	543.3[*,l] (6)	$31/2^{(-)} \rightarrow 29/2^-$	0.50 (20)	-	-		-
	701.3[*,m] (5)	$31/2^{(-)} \rightarrow (27/2^-)$	0.40 (20)	0.93 (12) [h]	-		($E2$)
4945.5 (8)	832.2[l] (5)	$(33/2^-) \rightarrow 29/2^-$	1.01 (30)		-		-
4952.9 (8)	858.4 (5)	$35/2^- \rightarrow 31/2^-$	1.48 (18)	0.92 (10)[f]	0.052 (40)		$E2$
	1347.0[l] (5)	$35/2^- \rightarrow 31/2^-$	0.50 (9)	-	-		-
5053.7 (9)	395.6[*,l] (6)	$(33/2^-) \rightarrow 31/2^{(-)}$	0.26 (20)	-	-		-
	748.1[l] (5)	$(33/2^-) \rightarrow 29/2^-$	-	-	-		-
5366.6 (10)	917.4[m] (5)	$37/2^{(-)} \rightarrow 33/2^-$	0.66 (9)	0.98 (8)[i]	-		($E2$)
5508.9 (9)	995.6 (4)	$39/2^- \rightarrow 35/2^-$	4.15 (34)	0.94 (8)[c]	0.037 (18)		$E2$
5932.2 (10)	979.3[m] (5)	$39/2^{(-)} \rightarrow 35/2^-$	0.33 (19)	0.95 (10)[f]	-		($E2$)
6381.8 (11)	1015.2[m] (6)	$41/2^{(-)} \rightarrow 37/2^{(-)}$	0.58 (7)	0.96 (10)[i]	-		($E2$)
6592.6 (10)	1083.7[m](4)	$43/2^{(-)} \rightarrow 39/2^-$	0.68 (11)	1.04 (10)[c]	-		($E2$)
7008.1 (11)	1075.9[m] (5)	$43/2^{(-)} \rightarrow 39/2^{(-)}$	0.31 (15)	1.11 (13)[f]	-		($E2$)
7662.6 (11)	1070.0[m] (6)	$47/2^{(-)} \rightarrow 43/2^{(-)}$	0.55 (32)	0.97 (16)[c]	-		($E2$)

The level energies are obtained by fitting the γ-ray energies using the RADWARE software.

† Intensities of γ-transitions are normalized to the 337.0 keV transition, with Iγ = 100.

$*$ Indicates new γ-transitions observed in the present work.

[a]DCO ratios are obtained by gating 745.9 keV stretched quadrupole ($E2$) transition.

[b]DCO ratios are obtained by gating 461.7 keV stretched quadrupole ($E2$) transition.

[c]DCO ratios are obtained by gating 337.0 keV stretched quadrupole ($E2$) transition.

[d]DCO ratios are obtained by gating 652.6 keV stretched quadrupole ($E2$) transition.

[e]DCO ratios are obtained by gating 607.1 keV stretched quadrupole ($E2$) transition.

[f]DCO ratios are obtained by gating 499.3 keV stretched quadrupole ($E2$) transition.

[g]DCO ratios are obtained by gating 701.2 keV stretched quadrupole ($E2$) transition.

[h]DCO ratios are obtained by gating 590.5 keV stretched quadrupole ($E2$) transition.

[i]DCO ratios are obtained by gating 706.3 keV stretched quadrupole ($E2$) transition.

[j]DCO ratios are obtained by gating 781.9 keV stretched quadrupole ($E2$) transition.

[k]DCO ratios are obtained by gating 670.1 keV stretched quadrupole ($E2$) transition.

[l]Multipolarity of these γ-transitions can not be determined due to very weak intensities.

[m]Δ_{asym} of these γ-transitions can not be determined due to weak intensity or contamination from the nearly same energies γ-transitions produced in the same nucleus.

[n]Multipolarity of these γ-transitions can not be determined due to the presence of very close Γ with energy 731.1-keV.

[o]Multipolarity of these γ-transitions can not be determined due to the strong contamination of 294.5 keV gamma.

[p]mixing ratios are calculated by using linear polarization and DCO values both.

[q] mixing ratios are calculated by using DCO values only.

[r]DCO ratios are obtained by gating 731.1 keV stretched quadrupole ($E2$) transition.

[s]DCO ratios are obtained by gating 520.7 keV stretched quadrupole ($E2$) transition.

The spectrums corresponding to newly observed gamma transitions are also shown in Fig. 6.4 and 6.5. Band 1 (erstwhile band 8) was proposed to be built on proton $h_{11/2}$ configuration and was suggested to be stabilized by $\beta \approx 0.21$, $\gamma \approx 11^{\circ}$ on the basis of results of TRS calculations. On the other hand, band 2 (earlier band 6) was found to evolve through a similar alignment of angular momentum as in band 1 and hence, based upon the energies of band 2, it was proposed to be the unfavored signature partner of band 1. Band 3 (erstwhile band 7) was proposed to be based on the γ vibration coupled to $h_{11/2}$ state. This conclusion was mainly based on similar alignment observed for bands 3 and 1, the same type of energy splitting was reported for the ground state and the $\alpha = 0$ sequence of the γ band in ^{120}Xe [199]. Later, Srebrny *et al.* probed the possibility of γ-softness resulting in wobbling dynamics in ^{119}I where band 1 was termed as $n_\omega = 0$ and band 2 was assigned to be $n_\omega = 1$ [200]. However, the assignment was fully based on Core-Quasiparticle Coupling

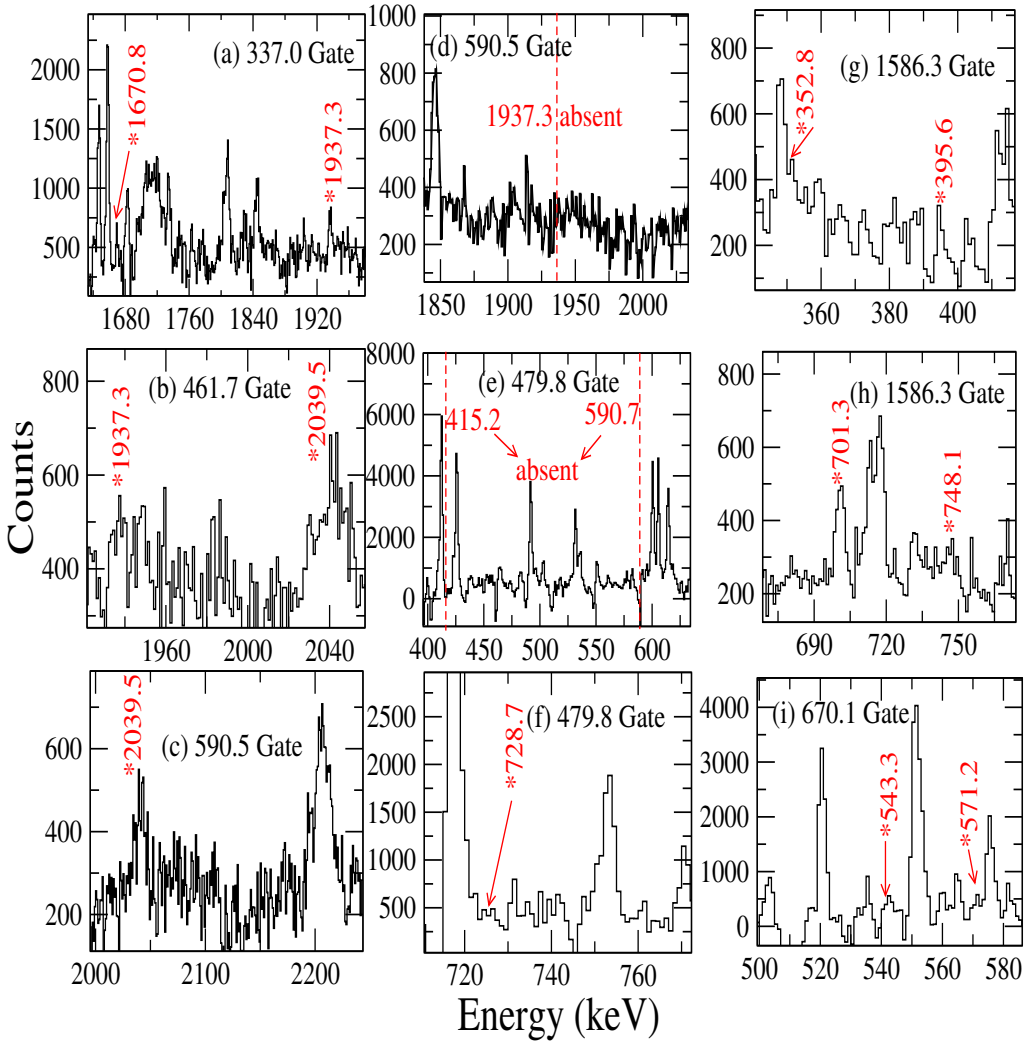

Figure 6.4 The γ-γ coincidence spectrum observed from the different gates to represent the newly observed transitions. An asterisk symbol shows the newly observed transitions.

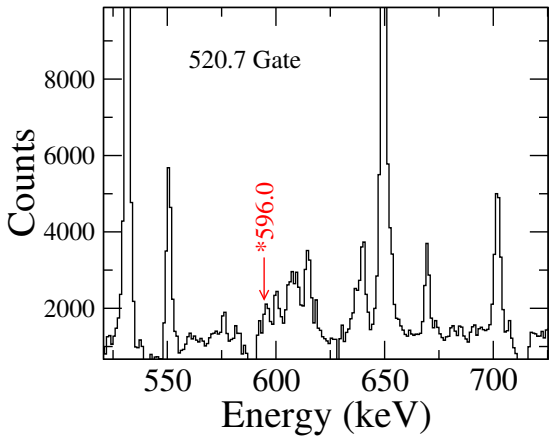

Figure 6.5 Figure shows the observation of 596.0-keV transition in the gate of 520.7-keV.

model with $h_{11/2}$ proton coupled to a collective quadrupole core. Therefore, it becomes intriguing to experimentally analyze the ^{119}I nucleus for the existence of wobbling motion.

To quantitatively determine the evolution of wobbling dynamics, one needs to confirm large mixing ratios of the $\Delta I = 1$ transitions interconnecting $n_\omega = 1$ and $n_\omega = 0$ as well as $n_\omega = 2$ and $n_\omega = 1$ along with the $\Delta I = 0$ transitions between the $n_\omega = 2$ and $n_\omega = 0$. At first, the interconnecting transitions between band 2 and band 1 were considered. The experimental value of a_2 and a_4 coefficients along with the theoretical values for 833.5- and 843.9-keV transitions are shown in Fig. 6.6 (a), (b), (c), and (d), respectively. The comparison of experimental a_2-a_4 values with the theoretical values based on standard χ^2 deviations for 833.5- and 843.9-keV transitions reveals an enhanced $E2$ fraction of 85.5% and 88.4%, respectively. It is to be mentioned that there are two nearly degenerate transitions with 851.8- and 851.2-keV energy. The 851.8-keV transition decays from $25/2^-$ of band 3 to $23/2^-$ of band 1. On the other hand, 851.2-keV γ ray transits from $21/2^-$ of band 2 to $19/2^-$ of band 1. It was not possible to resolve these two transitions within the experimental constraints, and hence, the angular distribution measurements could not be performed for the said transitions.

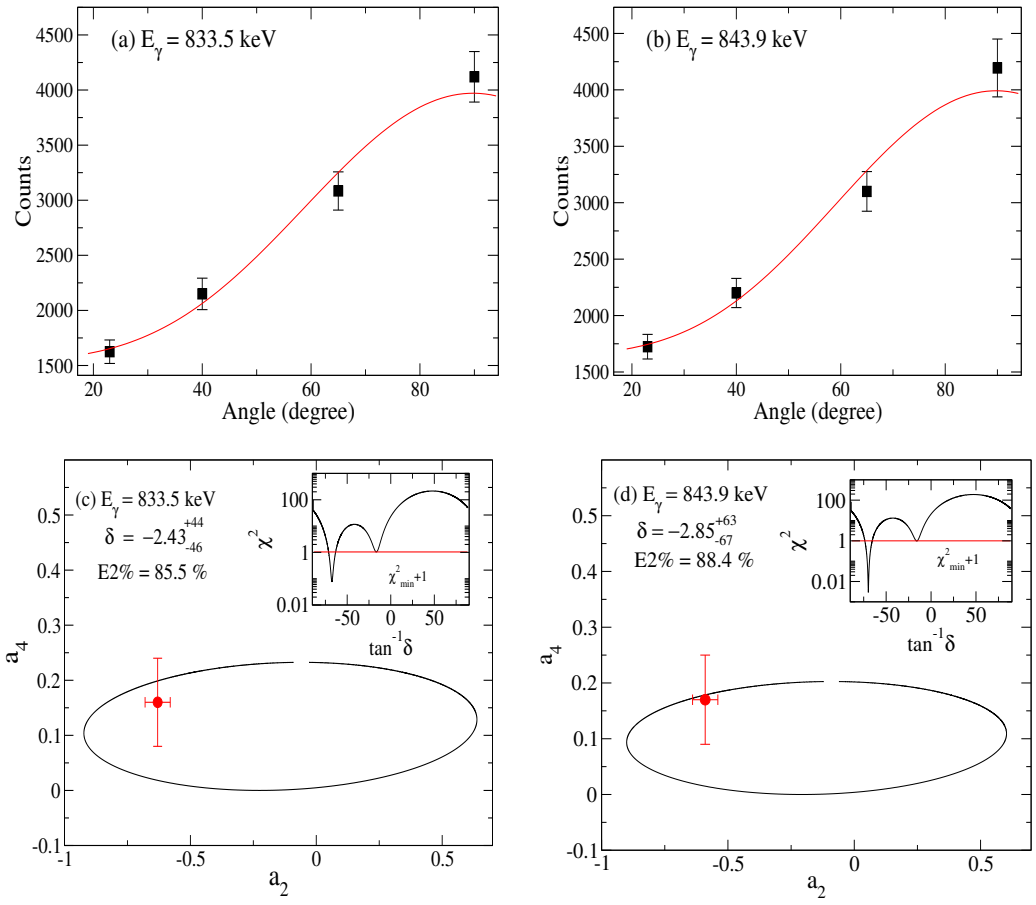

Figure 6.6 The panels (a) and (b) represent the angular distribution plots for the 833.5- and 843.9-keV transitions, respectively, in the gate of 337.0 keV ground state transition. The panels (c) and (d) represent the $a_2 - a_4$ plots for the 833.5- and 843.9-keV transitions, respectively. The experimental values are shown in red, which were obtained in the gate of 337.0 keV (ground state transition). The inset provides the χ^2 analysis for the experimental angular distribution of the corresponding transitions.

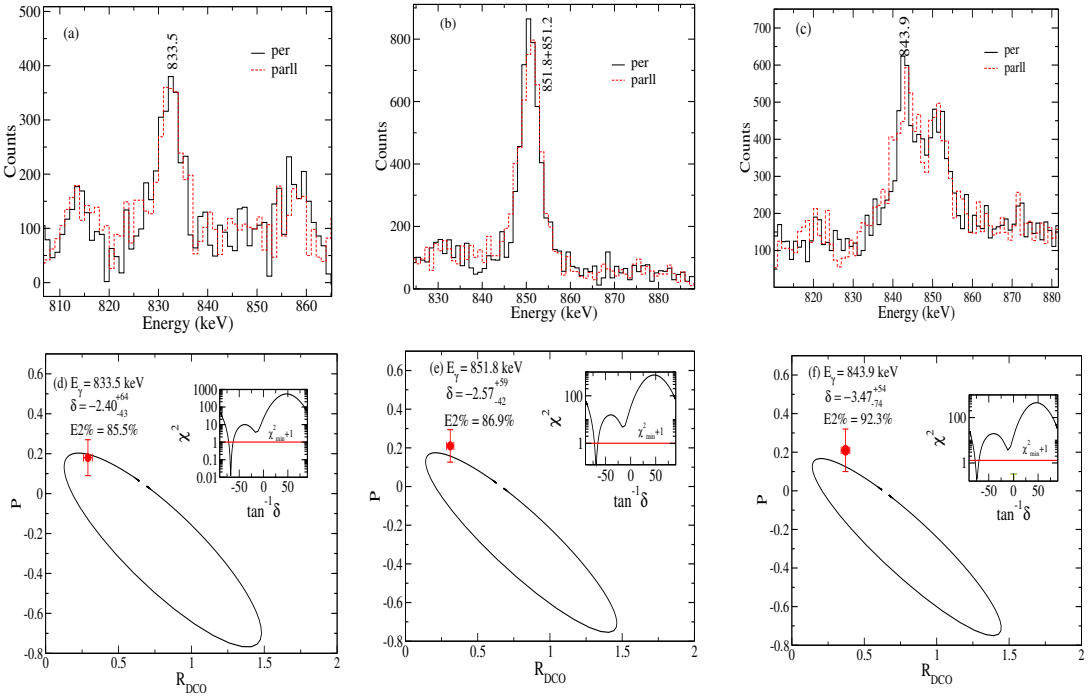

Figure 6.7 The panels (a), (b), and (c) represent the perpendicular and parallel spectrum for polarization. The corresponding gates are mentioned in the footnote of Table 6.2. The panels (d), (e), and (f) represent the R_{DCO} - P contour plots for the 833.5-, 851.8-, and 843.9-keV transitions. The inset provides the χ^2 analysis for the experimental R_{DCO} vs. P of the corresponding transitions.

To further justify the present findings, the R_{DCO}-polarization method has also been used to independently determine the mixing ratios and hence the $E2\%$ of the interconnecting transitions between bands 2 and 1. The gated spectra which have been used to extract the polarization for the 833.5-, (combined 851.2 and 851.8)- and 843.9-keV transitions are shown in Fig. 6.7 (a), (b), (c).

The contour plot of theoretical R_{DCO} and polarization along with the experimental values, are shown in Fig. 6.7 (d), (e), and (f). In the calculation of R_{DCO}, the width of the sub-state population (σ/j) was taken to be 0.3 [196]. The results confirm large $E2$ admixtures in 833.5-, 851.8-, and 843.9-keV transitions. The mixing ratios obtained from the R_{DCO}-Polarization method have been compared with the ones obtained from the

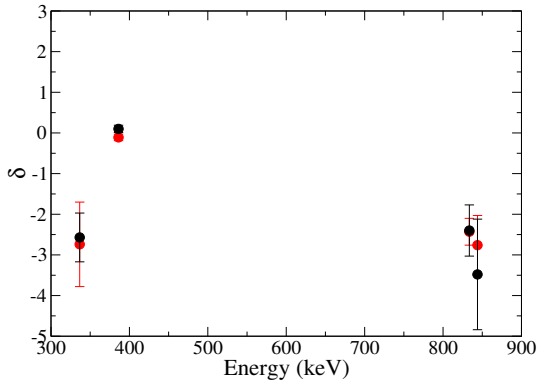

Figure 6.8 Comparison of δ values obtained from the angular distribution method and R_{DCO} vs. polarization method.

angular distribution method in Fig. 6.8 for the 833.5- and 843.9-keV connecting transitions, which confirms that the mixing ratios obtained from two different methods lie within the experimental uncertainties. The $E2$ fraction increases for the connecting transitions with increasing spin, indicating enhancement of wobbling with increasing angular momentum.

In order to confirm the $n_\omega = 2$ characteristics for band 2, the $\Delta I = 1$ transitions (decaying from band 2 to 1) 366.6 and 386.1 keV have been probed using the angular distribution method (see Fig. 6.9). The comparison of the experimental a_2 and a_4 with the theoretical values was used to extract $E2$ fraction. The $E2$ fraction for 366.6-keV transition was measured to be 88.8%, whereas surprisingly, the $E2$ admixture drops down to 1.2% for 386.1 keV.

To ascertain the sudden drop in $E2$% of 386.1-keV transition, the R_{DCO}-Polarization method was further applied to extract mixing ratios in an alternative way. The contour plots are shown in Fig. 6.10. The $E2$ admixture for 366.6- and 386.1-keV transitions agrees well with those found through the angular distribution method. It is further to be noted that the R_{DCO} value of 415.9 keV ($27/2^-$ of band 3 $\rightarrow$ $25/2^-$ of band 1) is measured to be 0.63, which indicates almost pure dipole transition, presumably $M1$. We have also

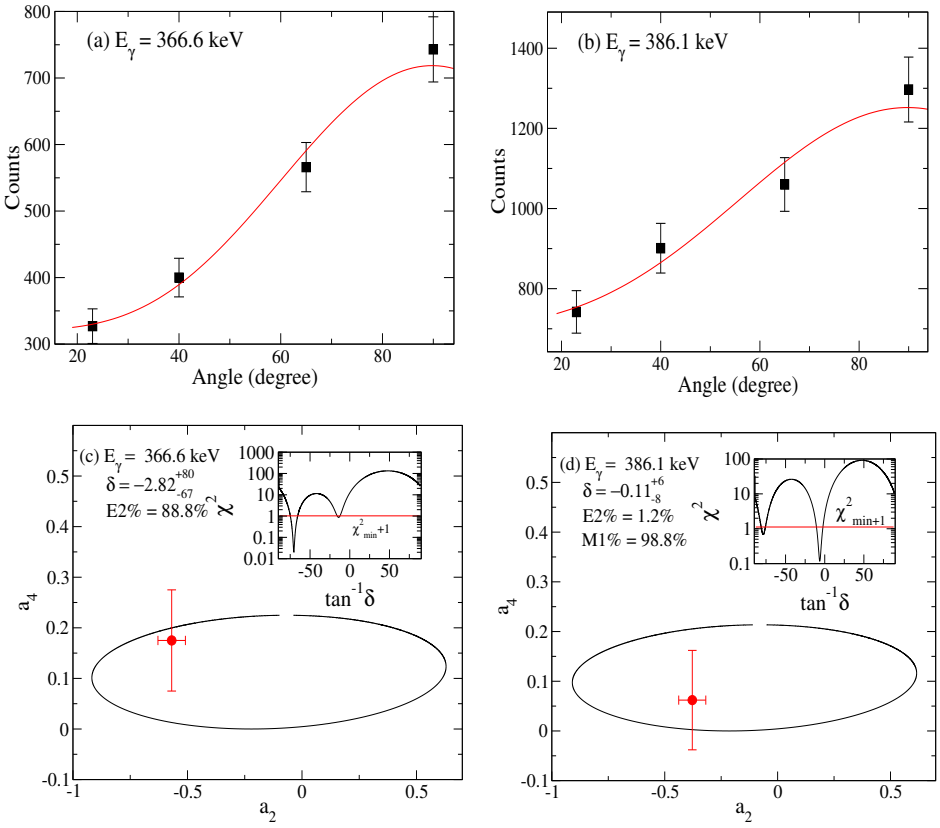

Figure 6.9 The panels (a) and (b) represent the angular distribution plot for 366.6- and 386.1-keV transitions in the gate of 499.3 and 461.7 keV transitions, respectively. The panels (c) and (d) represent the a_2 - a_4 contour plots of corresponding transitions. The inset provides the χ^2 analysis for the experimental angular distribution of the corresponding transitions.

measured the $E2\%$ of 738.2 keV transitions (feeding from the $19/2^-$ of band 3 $\rightarrow$ $19/2^-$ of band 1) and observed 72.3% of $E2$ admixture.

Hence, $\Delta I = 0$ 738.2 keV transition decaying from band 3 to band 1 shows a significant $E2\%$. However, only one such transition decaying from $I = 19/2^-$ in band 3 could be measured experimentally. On the other hand, for $\Delta I = 1$ transitions, large $E2$ admixture was only observed for one of the lowest transitions decaying from $I = 19/2^-$ in band 3. In contrast, transitions feeding from higher spins in band 3 to band 2 are mainly characterized by strong $M1$ contributions.

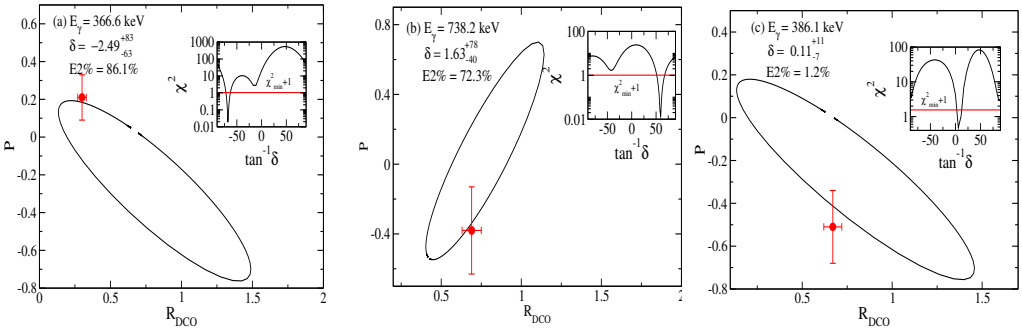

Figure 6.10 The panels (a), (b) and (c) represent the R_{DCO} - P contour plots for the 366.6-, 738.2 and 386.1 -keV transitions, respectively. The inset provides the χ^2 analysis for the experimental R_{DCO} vs. P values of the corresponding transitions.

Recently, the mixing ratios of inter-band γ-transitions have been extracted in several neutron-rich Mo, Ru, and Pd nuclei where γ-vibration bands were already reported. The observed results indicate a decline in $E2\%$ with the increase in angular momentum for $\Delta I = 0$ transitions decaying from the γ-band to the ground band. However, in the present study, there are only two $\Delta I = 0$ transitions decaying from band 3 to 1, out of which the $E2$ fraction of only one transition *i.e.*, 738.2 keV can be extracted. Therefore, it is difficult to conclude that band 3 can be designated as γ-band.

The observation of several $\Delta I = 1, 2$ transitions from bands 3 to 2 and 3 to 1 suggests that this band can stand as the $n_\omega = 2$ band as reported in the case of ^{125,127}Xe, ^{163,165}Lu, ^{133}Ba, and ^{135}Pr. In the case of $n_\omega = 2$ band, a large $E2\%$ is expected between the $\Delta I = 1$ transitions decaying from $n_\omega = 2$ to $n_\omega = 1$ band. However, in the present work, the $E2\%$ sudden decrease at level $23/2^-$. Thus, the interpretation of band 3 as an $n_\omega = 2$ band does not appear to be feasible. Since the decay pattern of band 3 is similar to both $n_\omega = 2$ band and the even spin member of the γ-vibration band, the observed features of this band may suggest a coupling between the wobbling dynamics and the γ-vibration. Such a coupling mechanism has also been theoretically predicted in ^{164}Hf through self-consistent calculations employing the tilted-axis cranking model. A comprehensive understanding of

band 3 may be obtained through a detailed investigation of its nature within an appropriate theoretical framework.

Table 6.3 Measured B$(E2)_{out}$/B$(E2)_{in}$ and B$(M1)_{out}$/B$(E2)_{in}$ values of interconnecting transitions from band 2 to 1 and 3 to 2 in ^{119}I.

$E\gamma$ (keV)	$I_i \rightarrow I_f$	B$(E2)_{out}$/B$(E2)_{in}$	B$(M1)_{out}$/B$(E2)_{in}$ $(\frac{\mu_N^2}{e^2b^2})$
843.9	$29/2^- \rightarrow 27/2^-$	0.29 (4)	0.011 (4)
366.6	$19/2^- \rightarrow 17/2^-$	0.98 (33)	0.014 (8)
386.1	$23/2^- \rightarrow 21/2^-$	0.013 (2)	0.12 (10)
415.9	$27/2^- \rightarrow 25/2^-$	0.020 (4)	0.20 (17)

The reduced transition probability ratios B$(E2)_{out}$/B$(E2)_{in}$ and B$(M1)_{out}$/B$(E2)_{in}$ were also measured to determine the $E2$ character of the linking transitions. These ratios are summarized in Table 6.3. The large B$(E2)_{out}$/B$(E2)_{in}$ values of 843.9- and 366.6-keV traditions also support the predominant $E2$ character of the linking transitions, whereas 386.1 and 415.9-keV transitions have large values of B$(M1)_{out}$/B$(E2)_{in}$ which show the predominant $M1$ character. [47, 54, 56, 196].

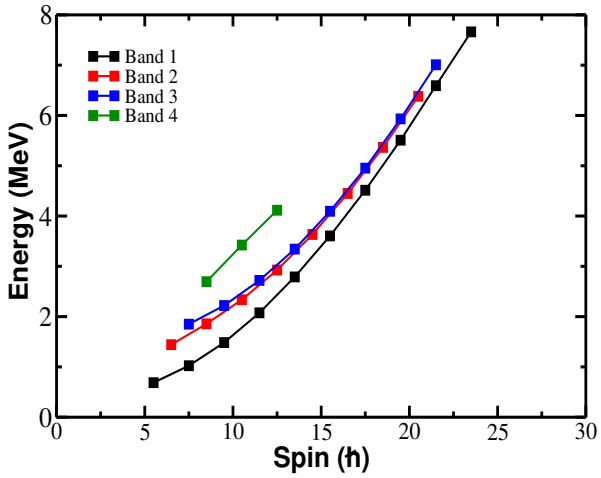

Figure 6.11 Excitation energies as a function of spin of bands 1, 2, 3, and 4 in ^{119}I.

In the case of odd-A nuclei, a signature partner band of $n_\omega = 0$ is also expected to exist. The signature partner band is supposed to be located at higher energies compared

to the $n_\omega = 0, 1$, and 2, because it originates when the angular momentum of odd particle is aligned away from the principal axes [54, 56, 191]. Since the $n_\omega = 0$ band is based on low$-\Omega\pi(h_{11/2})$ orbitals, a large signature splitting can be expected between the favored and unfavored signature partners. In the present work, three new gamma transitions with 1670.8, 1937.3, and 2039.5 keV higher energies were observed. The levels from which these γ transitions decay are grouped as band 4. The measured R_{DCO} values of 1670.8- and 1937.3-keV transitions are 0.66 (5) and 0.63 (5), respectively, which represent the dipole character of these transitions. Hence, band 4 can stand as the signature partner band of $n_\omega = 0$ band. Due to the very weak intensities of these transitions, polarization measurements are not possible in the present work. In Fig. 6.11 excitation energy versus spin has been depicted for the assumed signature partner band of ^{119}I.

The E_{wobb} energy has been measured for ^{119}I and it was observed that the E_{wobb} decreases as the spin increases, indicating the alignment of angular momentum of odd particles along long or short axes, generally known as transverse wobbler. E_{wobb} with respect to spin has been plotted for different nuclei in Fig. 6.12, where the transverse wobbling motion is reported along with the ^{119}I.

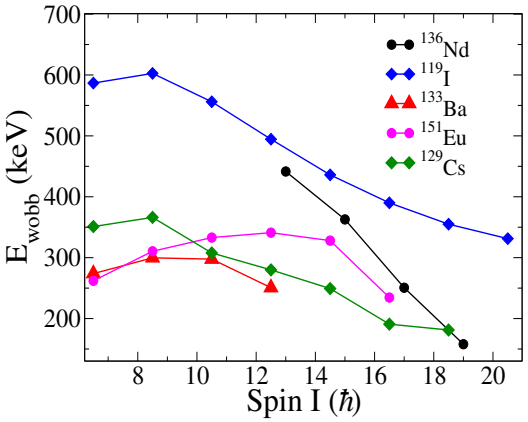

Figure 6.12 Experimentally observed E_{wobb} energies with respect to spin for ^{119}I, ^{136}Nd, ^{133}Ba, ^{151}Eu and ^{129}Cs.

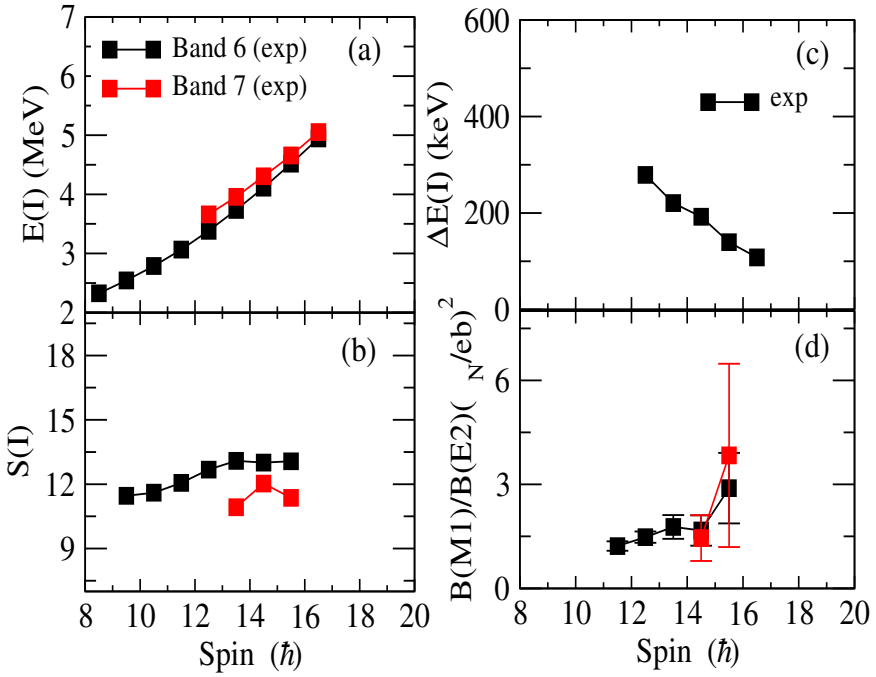

Figure 6.13 Figures (a), (b), (c), and (d) represent the experimental values of excitation energies, staggering parameter, energy difference, and transition probability ratios with respect to spin, respectively between bands 6 and 7.

Further, the structure of bands 6 and 7 looks to originate from the chiral symmetry breaking. Band 6 was reported to be based on the configuration $\pi g_{9/2} \nu h_{11/2} g_{7/2}$ [189]. The existence of similar type of $\Delta I = 1$, $M1$/ $E2$ and $E2$ transitions in band 7 and also the observation of $\Delta I = 1$ linking transitions between bands 6 and 7 implies that band 7 should have the same intrinsic configuration $\pi g_{9/2} \nu h_{11/2} g_{7/2}$ as band 6. To investigate whether these bands are associated with chiral symmetry, we have extracted some parameters, such as excitation energies $E(I)$, staggering parameter $S(I)$, energy separation, and B($M1$)/B($E2$) for both bands which are the signatures of the chirality (see Fig. 6.13). It was observed that both bands show similar types of excitation energies, smooth variation of $S(I)$, and almost the same B($M1$)/B($E2$) values for the $\Delta I = 1$ transitions with respect to spin as expected for chiral partner bands. The energy separation between these bands decreases as the spin

increases, which indicates the transformation from chiral vibration to static chirality as observed in ^{135}Nd [37].

6.4 Summary

The negative parity states of ^{119}I based on $\pi h_{11/2}$ have been revisited. Band 2 has been established as a first phonon wobbling band based on large $E2\%$ of interconnecting ΔI = 1 transitions between bands 2 and 1. Band 3 was observed to show some anomalous behavior at spin $19/2^-$; the $E2\%$ of ΔI = 1, 0 are observed to be very high, while after spin $19/2^-$, a sudden drop in $E2\%$ (of the order of 1%) of ΔI = 1 transition is observed. The clear evidence of its nature could not be determined in this work. The n_ω = 0 band is based on low Ω orbitals, so its signature partner band can be expected to be at a higher energy. Three new gamma transitions with 1670.8, 1937.3, and 2039.5 keV higher energies were observed to decay at n_ω = 0. The levels from which these γ transitions decay are grouped as band 4 and are supposed to be the signature partner band of n_ω = 0 band based on the $M1$ character of those transitions. Further, bands 6 and 7 are assigned as chiral partner bands based on the same type of excitation energies $E(I)$, staggering parameter $S(I)$, and B($M1$)/B($E2$) values.